

Supporting Information

Liquid Organic Frameworks: The Single Network “Plumber’s Nightmare” Bicontinuous Cubic Liquid Crystal

Silvio Poppe^a, Xiaohong Cheng^{a,b}, Changlong Chen^c, Xiangbing Zeng,^d Rui-bin Zhang,^d Feng Liu^{c,*}, Goran Ungar^{c,d,*}, Carsten Tschierske^{a,*}

^a Institute of Chemistry, Martin-Luther-University Halle-Wittenberg, Kurt-Mothes-Straße 2, 06120 Halle, Germany

^b Key Laboratory of Medicinal Chemistry for Natural Resources, Chemistry Department, Yunnan University, Kunming 650091, P. R. China

^c State Key Laboratory for Mechanical Behaviour of Materials, Shaanxi International Research Center for Soft Matter, Xi’an Jiaotong University, Xi’an 710049, P. R. China

^d Department of Materials Science and Engineering, University of Sheffield, Sheffield S1 3JD, U.K.

Contents

S1. Experimental Methods	2
S1.1. Optical and calorimetric investigations	2
S1.2. X-ray diffraction	2
S1.3. Atomic force microscopy	3
S2. Additional experimental data	3
S3. Analysis of X-ray data	5
S3.1. Electron density reconstruction	5
S3.2. Simulation of XRD intensities	7
S4. Synthesis and analytical data	10
S4.1 General procedures	10
S4.2 Synthesis of compound 2	11
S4.3. Synthesis of compound 3	15
S5. Supporting Discussion and Calculations	16
S5.1 Difference between molecular length and a_{cub}	16
S5.2 Packing of R_{F} chains in the $Pm3m$ phase of compound 2	17
S6. Additional NMR spectra	18
S7. References	21

S1. Experimental Methods

Moisture control. Because the investigated amphiphilic compounds with glycerol groups can contain water in the crystalline state^{S1} and easily take up water in the LC state the samples were rigorously dried before investigation. For this purpose the samples were heated into the Iso state at least 20 K above the LC-Iso transition temperature, but at least to 150 °C for about 1 minute. This treatment removes all water (and possible remaining traces of solvent from chromatography and crystallization) as proven previously.^{S2} The used capillaries, microscopy glass plates and DSC pans were heated for 20 min in a vacuum oven to 200 °C before use. The samples were immediately sealed and investigated. Polarizing microscopy was conducted in the center of the sample.

S1.1. Optical and calorimetric investigations

Phase transitions were determined by polarizing microscopy (Leica DMR XP) in conjunction with a heating stage (FP 82 HT, Mettler) and controller (FP 90, Mettler) and by differential scanning calorimetry (DSC-7, Perkin Elmer) at heating/cooling rates of 10 K min⁻¹ (peak temperatures). Optical investigation was carried out under equilibrium conditions between glass slides, sample thickness was ~15 μm. A full wavelength retardation plate was used to determine the sign of birefringence. Optical micrographs were taken using a Leica MC120HD camera.

S1.2. X-ray diffraction

Laboratory X-ray experiments. X-ray investigations (Kristalloflex 760H, Siemens) were carried out using Ni filtered CuK α radiation (15 to 30 min exposure time). The samples were heated to isotropic state and filled in thin capillaries ($\phi = 1$ mm). Afterwards the capillaries were sealed. The samples were held on a temperature controlled heating stage and the diffraction patterns were recorded with a 2D detector (Vantec 500, Bruker). For the measurement the samples were heated to isotropic state and slowly cooled to the LC state. The sample-detector distance for the samples was 9.00 cm for WAXD and 26.70 cm for SAXD measurements.

Synchrotron X-ray experiments. High-resolution small-angle powder diffraction experiments were recorded on Beamlines BL16B1 at Shanghai Synchrotron Radiation Facility (SSRF) and Beamline I22 at Diamond Light Source. Samples were held in evacuated 1 mm capillaries. A modified Linkam hot stage with a thermal stability within 0.2 °C was used, with a hole for the capillary drilled through the silver heating block and mica windows attached to it on each side. q calibration and linearization were verified using several orders of layer reflections from silver behenate and a series of n -alkanes. A Pilatus detector was used for SAXS.

GISAXS experiments were carried out on Beamlines BL16B1 at SSRF and station BM28 (XMaS line) at ESRF. Thin films were prepared from the melt on a silicon wafer. The thin film coated $5 \times 5 \text{ mm}^2$ Si plates were placed on top of a custom built heater, which was then mounted on a six-circle goniometer. A Pilatus detector at SSRF and a MarCCD 165 detector at ESRF was used. The sample enclosure and the beam pipe were flushed with helium.

S1.3. Atomic force microscopy

Tapping mode AFM experiment was carried out on a Multimode 8 instrument (Bruker) with a Nanoscope V controller. Hi'Res-C probes from MikroMasch were used for the scanning. The sample film on silicon surface was drop-cast from a 5 mg/ml THF solution, which was then dried in a vacuum oven for 2 hours. Prior to scanning the sample was heated into the cubic phase at 140°C , then rapidly cooled to 80°C and scanned immediately, using a high-temperature J-scanner. This procedure ensured that the compound is kept in the cubic phase while maintaining high resolution.

S2. Additional experimental data

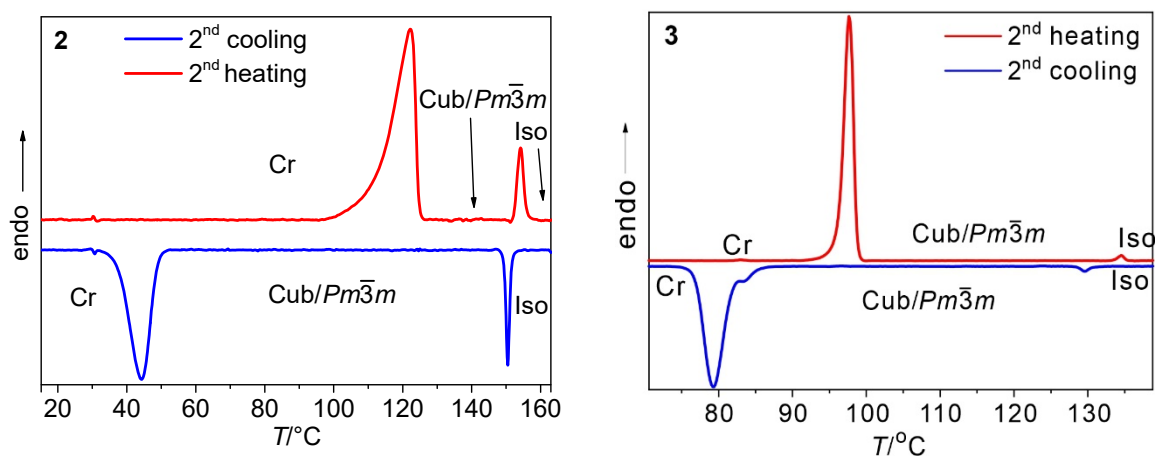


Figure S1. DSC traces of compounds **2** and **3** recorded at 10 K min^{-1} .

Table S1. Experimental and calculated d -spacings of the observed SAXS reflections of the Cub/ $Pm\bar{3}m$ phases of compounds **2** and **3**, all intensity values are Lorentz corrected with correction for multiplicity.

Compd.	(hkl)	$d_{\text{obs.}}$ (nm)	$d_{\text{cal.}}$ (nm)	Intensity	phase	a_{cub} ($T/^\circ\text{C}$)
2	(100)	2.89	2.89	100.0	π	2.89 nm (150 °C)
	(110)	2.04	2.04	2.0	0	
	(111)	1.67	1.67	89.2	0	
	(200)	1.45	1.45	7.1	0	
	(210)	1.30	1.29	4.8	0	
	(300)	0.97	0.96	4.6	π	
3	(100)	3.61	3.61	100.0	0	3.61 nm (100 °C)
	(110)	2.56	2.55	0.1	0	
	(111)	2.09	2.08	5.6	π	
	(200)	1.81	1.81	3.2	0	
	(210)	1.62	1.61	0.1	π	

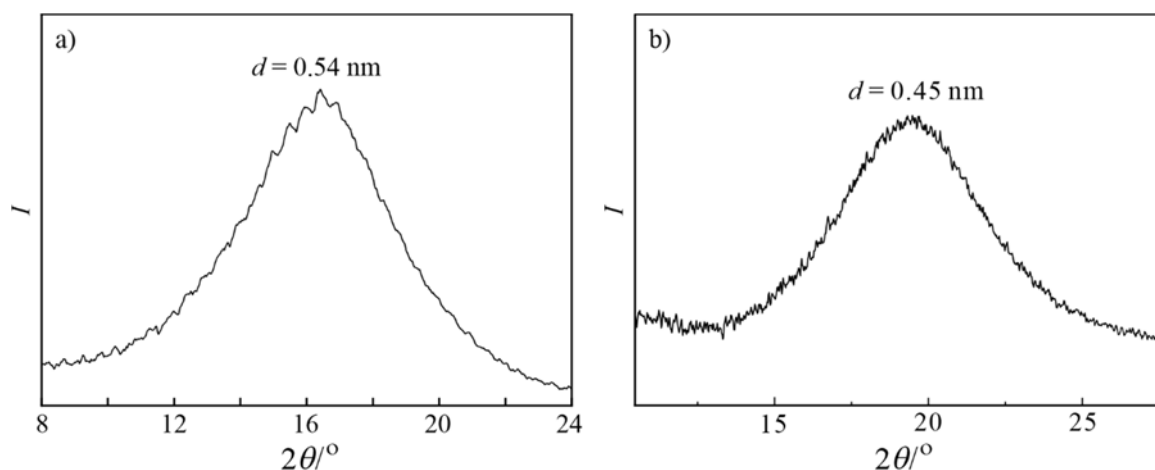


Figure S2. WAXS diffractogram of the Cub/ $Pm\bar{3}m$ phase of **2** at $T = 150\text{ }^\circ\text{C}$ (a) and **3** at $T = 100\text{ }^\circ\text{C}$ (b).

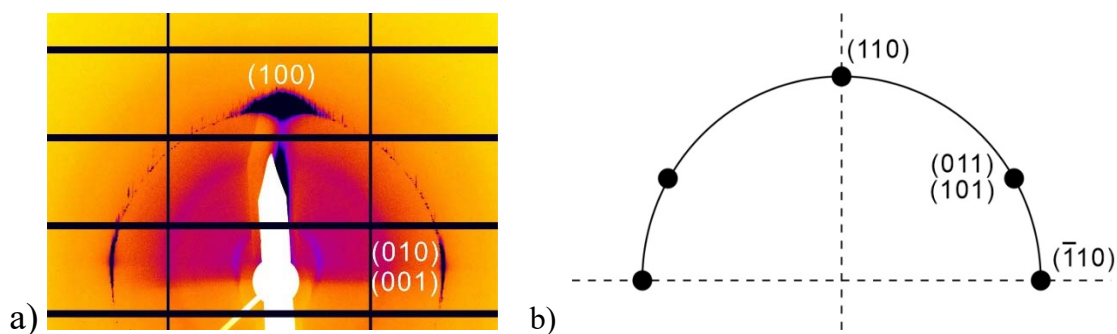


Figure S3. (a) Experimental GISAXS pattern of the Cub/ $Pm\bar{3}m$ phase of **3** at $T = 110$ °C; (b) simulated GISAXS pattern of the Cub/ $Im\bar{3}m$ phase, the (110) direction of the Cub/ $Im\bar{3}m$ phase is normal to the substrate surface.

Table S2. Structural data for the Cub/ $Pm\bar{3}m$ phases of compounds **2** and **3**.

Compd.	a [nm]	$V_{\text{mol}}/[\text{nm}^3]$	$V_{\text{cell}}/[\text{nm}^3]$	n_{cell}	n_{bundle}	d_{nodes}
2	2.89	1.13	24.39	19.27	6.42	2.89
3	3.61	1.60	47.44	26.47	8.82	3.61

V_{mol} was determined using the volume increments by Immirzi^{S3}, $V_{\text{cell}} = a^3$ for cubic lattice, $n_{\text{cell}} = 0.893 \cdot (V_{\text{cell}}/V_{\text{mol}})$, number of molecules within one unit cell, n_{bundle} – number of molecules forming one molecular bundle, d_{nodes} – distance between two adjacent spheres in cubic phases.

S3. Analysis of X-ray data

S3.1. Electron density reconstruction

The diffraction peaks are indexed on the basis of their d -spacing ratio, and the lattice parameters and the space groups are subsequently determined. Once the diffraction intensities are measured and the corresponding space group determined, 3-d electron density maps could be reconstructed, on the basis of the general formula

$$E(xyz) = \sum_{hkl} F(hkl) \exp[i2\pi(hx+ky+lz)] \quad (\text{Eqn. 1})$$

Here $F(hkl)$ is the structure factor of a diffraction peak with index (hkl) . It is normally a complex number and the experimentally observed diffraction intensity

$$I(hkl) = K \cdot F(hkl) \cdot F^*(hkl) = K \cdot |F(hkl)|^2 \quad (\text{Eqn. 2})$$

Here K is a constant related to the sample volume, incident beam intensity etc. Here we are only interested in the relative electron densities, hence this constant is simply taken to be 1. Thus the electron density is

$$E(xyz) = \sum_{hkl} \text{sqrt}[I(hkl)] \exp[i2\pi(hx+ky+lz) + \phi_{hkl}] \quad (\text{Eqn. 3})$$

As the observed diffraction intensity $I(hkl)$ is only related to the amplitude of the structure factor $|F(hkl)|$, the information about the phase of $F(hkl)$, ϕ_{hkl} , can not be determined directly from experiment. However, the problem is much simplified when the structure of the ordered phase

is centrosymmetric, and hence the structure factor $F(hkl)$ is always real and ϕ_{hkl} is either 0 or π . This makes it possible for a trial-and-error approach, where candidate electron density maps are reconstructed for all possible phase combinations, and the “correct” phase combination is then selected on the merit of the maps, helped by prior physical and chemical information on the system.

In this work the initially determined maps, combined with prior knowledge of molecular dimensions and volumes, already hinted strongly at the model of the type depicted in Figure 3f. Hence a mathematical model was built representing it, as described in Section S3.2, and the final phase choice for calculating the electron density maps was obtained from Fourier series development of the model. The maps are represented by isoelectron surfaces at two levels in Fig. 3c,g and at multiple levels in Fig. S4. Histograms of volume fraction vs. electron density are shown in Fig. S5.

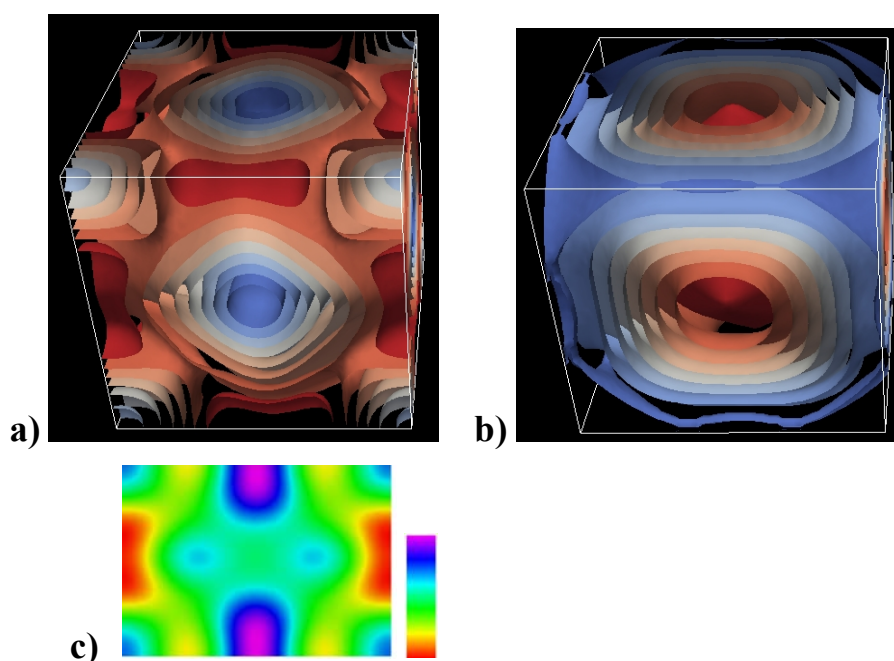


Figure S4. Multilevel electron density maps of (a) compound **2** and (b) compound **3** reconstructed based on the phase combinations obtained from Fourier representation of the models in Figures 3d and 3h, respectively. Colour scale: blue = high, red = low. (c) The (110) (diagonal) section of the ED map of **2** with its colour scale. The purple blobs are the fluoroalkyl clusters at the top and bottom face centres, the red minima are the terphenyls with and the light-blue maxima at the corners are the glycerols. Note the local minimum in the body centre (green) where the side-chains must stretch to reach.

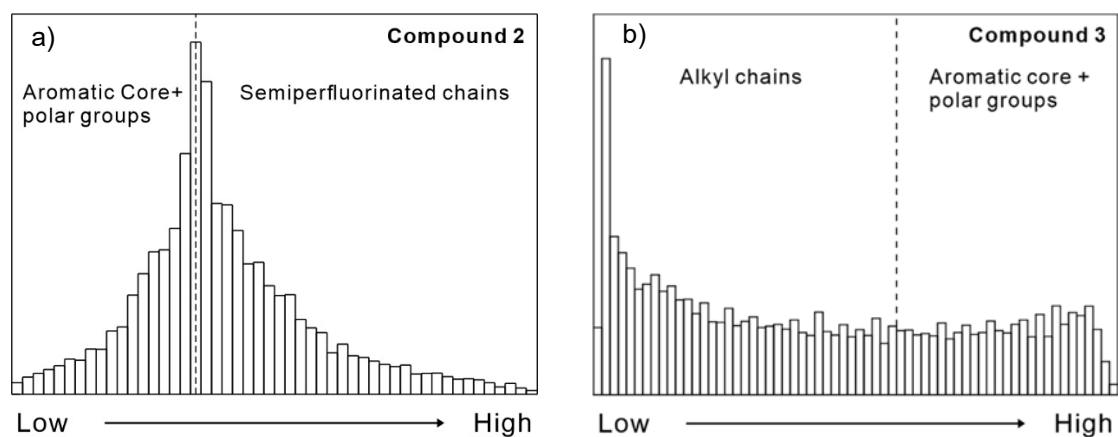


Figure S5. Volume fraction vs. electron density histograms of the Cub/ $Pm\bar{3}m$ phase of compounds (a) **2** and (b) **3** calculated from the electron density maps in Figures 3c and 3g. The calculated subphase volume ratios are 0.44:0.56 for (aromatic + glycerol) groups and semiperfluorinated chains of compound **2**, and 0.64:0.36 for alkyl chains and (aromatic + glycerol) groups of compound **3**, respectively (see dashed vertical subphase demarcation lines).

S3.2. Simulation of XRD intensities

Geometrical models of the cubic phases formed by compounds **2** and **3** have been built for simulation of their diffraction intensities. Starting with the simpler case of compound **3**, the regions occupied by aromatic backbones are represented by square columns along the edges of the unit cell, and those occupied by the polar glycerol groups by truncated octahedra (cubooctahedra) at cell corners. The model is shown in Figure S6e and Figure 3h of the main text. The parameter p of the model, defining the thickness of the columns and the size of the cubooctahedra (see Figure S6e) is chosen such that $0.283a = 1.02$ nm, so that the total volume of the aromatic and polar groups is 36% of the unit cell volume, as estimated using the volume increments method by Immirzi.^{S3} The electron densities of polar groups (0.45 e/Å³), aromatic groups (0.40 e/Å³) and aliphatic groups (0.33 e/Å³) have also been calculated by volume increments. Taking aliphatic regions as the background, we have the relative electron density of the polar groups $\rho_{\text{polar}} = 0.12$ e/Å³, and that of the aromatic groups $\rho_{\text{arom}} = 0.07$ e/Å³.

The Fourier transform of an octahedron with a uniform density of 1, centred at (0,0,0) and one of its corners at $(u,0,0)$ (Figure S6a), can be written as

$$F_{\text{Oct}}(q_x, q_y, q_z, u) = 8 \left[\frac{q_x \sin(q_x u)}{(q_x^2 - q_y^2)(q_z^2 - q_x^2)} + \frac{q_y \sin(q_y u)}{(q_x^2 - q_y^2)(q_y^2 - q_z^2)} + \frac{q_z \sin(q_z u)}{(q_y^2 - q_z^2)(q_z^2 - q_x^2)} \right]$$

The Fourier transform of a truncated octahedron as shown in Figure S5b would be

$$\begin{aligned} F_{t\text{-Oct}}(q_x, q_y, q_z, u, v) \\ = F_{\text{Oct}}(q_x, q_y, q_z, u + v) - F_{\text{Oct}}(q_x, q_y, q_z, v) [\cos(q_x u) + \cos(q_y u) \\ + \cos(q_z u)] \end{aligned}$$

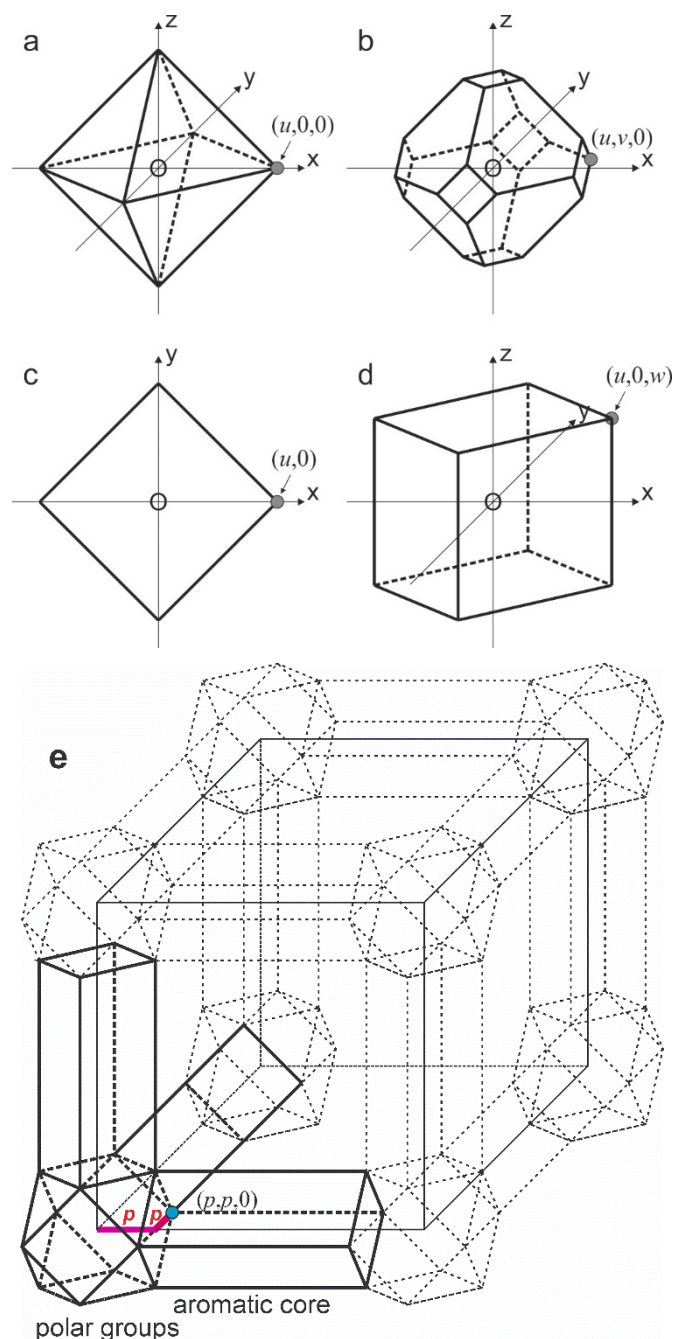


Figure S6. (a) Octahedron. (b) Truncated octahedron. (c) Square. (d) Square column. (e) Model of a unit cell of compound 3, as in Fig. 3h but with a definition of parameter p .

The Fourier transform of a square (Figure S6c) is

$$F_{\text{square}}(q_x, q_y, u) = 8 \frac{\sin\left[\frac{(q_x + q_y)u}{2}\right] \sin\left[\frac{(q_x - q_y)u}{2}\right]}{q_x^2 - q_y^2}$$

The Fourier transform of a square column (Figure S6d) is

$$F_{\text{sq-col}}(q_x, q_y, q_z, u, w) = F_{\text{square}}(q_x, q_y, u) \frac{\sin(q_z w)}{q_z}$$

Therefore, the structure factor of this three-level model of the $Pm\bar{3}m$ phase of compound 3 can be written as

$$\begin{aligned}
F_{3-level} = & \rho_{polar} F_{t-oct}(q_x, q_y, q_z, p, p) \\
& + \rho_{arom} \left[F_{sq-col}(q_y, q_z, q_x, p, 0.5 - p) \cos\left(\frac{q_x}{2}\right) \right. \\
& + F_{sq-col}(q_x, q_z, q_y, p, 0.5 - p) \cos\left(\frac{q_y}{2}\right) \\
& \left. + F_{sq-col}(q_x, q_y, q_z, p, 0.5 - p) \cos\left(\frac{q_z}{2}\right) \right]
\end{aligned}$$

The diffraction intensities (which are proportional to $|F|^2$) and structure factor phases of different diffraction peaks can thus be calculated and are listed in Table S3. The experimental and simulated intensities are compared in Fig. 3e.

Table S3. Diffraction indices, measured and calculated diffraction intensities, and phases retrieved from simulation of compound **3**, using the geometrical model shown in Figure 3h.

(hkl)	Intensities (exper.)	Intensities (simulated)	Phase (simulated)
(100)	100.0	98.7	0
(110)	0.1	0.9	0
(111)	5.6	9.5	π
(200)	3.2	11.5	0
(210)	0.1	0.2	π

For the simulation of X-ray diffraction intensities of compound **2**, in addition to the aliphatic, polar and aromatic groups, the contribution from the perfluorinated segments of the side chains, which have the highest electron density (absolute $0.66 \text{ e}/\text{\AA}^3$, relative $\rho_F = 0.33 \text{ e}/\text{\AA}^3$) must be added. The region occupied by the fluorinated group is represented by another octahedron centred at the body-centre of the unit cell which is this time truncated by the faces of the cubic unit cell or, in other words, by collision with the octahedra from neighbouring cells. Like for compound **3**, the model parameter p is chosen as $p = 0.327a = 0.95 \text{ nm}$ so that the polar + aromatic volume equals 45% of the total volume (calculated by volume increments). The size of the fluorinated octahedron is defined by parameter v , the half-diagonal of the truncating square faces. v , and thus the size of the central octahedron, was used as the fitting parameter. The best fitting value of v is found to be $v = 0.112a = 0.32 \text{ nm}$, corresponding to the fluorinated octahedron occupying 30% of the total volume and not far from the calculated fluoroalkyl volume fraction of 41%. The structure factor of the new four-level model is

$$F_{4-level} = F_{2-level} + \rho_F F_{t-oct}(q_x, q_y, q_z, 0.5, v) \cos\left[\frac{q_x + q_y + q_z}{2}\right]$$

Calculated diffraction intensities, which are proportional to $|F|^2$, and structure factor phases for compound **2** are listed and compared to experimental ones in Table S4 and Fig. 3a.

Table S4. Diffraction indices, measured and calculated diffraction intensities, and phases retrieved from simulation of compound **2**, using the geometrical model shown in Figure 3d.

<i>(hkl)</i>	Intensities (exper.)	Intensities (simulated)	Phase (simulated)
(100)	100	97.8	π
(110)	2	13.0	0
(111)	89.2	89.4	0
(200)	7.1	11.6	0
(210)	4.8	1.3	0
(211)	0	3.0	π
(220)	0	0.1	π
(300)*	4.6*	2.5	π
(221)*	0*	0.4	0

* Experimentally cannot be differentiated from powder diffraction, attributed to (300) only.

S4. Synthesis and analytical data

S4.1 General procedures

Unless otherwise noted, all starting materials were purchased from commercial sources and were used without further purification. Column chromatography was performed with silica gel 60 (63-200 μm , Fluka). Determination of structures and purity of intermediates and products was obtained by NMR spectroscopy (VARIAN Gemini 2000 and Unity Inova 500, all spectra were recorded at 27 °C). Microanalyses were performed using a CARLO Erba-CHNO 1102 elemental analyzer and a microTOF HR-ESI mass spectrometer (Bruker). The purity of all products was checked with thin layer chromatography (silicagel 60 F₂₅₄, Merck). CHCl₃ and CHCl₃/MeOH mixtures were used as eluents and the spots were detected by UV radiation. C_nH_{2n+1} represent linear chains. The synthesis of 1,4-diodo-2,3-dialkoxybenzenes is described in ref.^{S 4}. 4-[(2,2-Dimethyl-1,3-dioxolane-4-yl)methoxy]phenylacetylene (**4**) and 4-((2,2-dimethyl-1,3-dioxolane-4-yl)methoxy)benzeneboronic acid were synthesized according to refs.^{S 5,S 6} 2-Pentylheptylbromide was synthesized as reported in ref.^{S 5} 3-Allylanisole was synthesized as reported in ref.^{S 7} 3-Bromoanisole and 1,4-benzenediboronic acid were purchased commercially und were used without further purification.

MHz; CDCl₃): δ / ppm = 7.28 (m, 1H, Ar-*H*), 6.86 (m, 3H, Ar-*H*), 4.49 (m, 1H, *CHI*), 3.84 (s, 3H, *CH*₃), 3.25 (m, 2H, Ar*CH*₂), 2.98 (m, 2H, *CH*₂).

3-(1H,1H,2H,2H,3H,3H-Perfluorononyl)anisole 5. To a slurry of LiAlH₄ (2.50 g, 65.8 mmol) in dry Et₂O (100 mL), 3-(1H,1H,2H,3H,3H-perfluoro-2-iodononyl)anisole (36.40 g, 61.3 mmol) dissolved in dry diethyl ether (100 mL) was added dropwise to maintain the solution at reflux. The mixture was refluxed for further 2 h, and cooled to RT. Afterwards, water was added dropwise until all the unreacted LiAlH₄ was decomposed. Then 50 % aqueous H₂SO₄ was carefully added to dissolve the solid. The organic layer was separated and the aqueous layer was extracted with Et₂O (3×150 mL), the organic layers were combined and washed with 10 % aqueous Na₂S₂O₃ till the aqueous layer remained colorless. After being washed further with H₂O (2×100 mL) and brine (2×100 mL) and dried over Na₂SO₄, the solvent was removed in *vacuo*, the oily residue was distilled in *vacuo*. yield: 13.7 g (47.7 %); yellow oil; bp: 84 °C / 0.18 mbar; C₁₆H₁₃OF₁₃, M = 468 g/mol, ¹H-NMR (200 MHz; CDCl₃): δ / ppm = 7.29 (m, 1 H, Ar-*H*), 6.79 (m, 3 H, Ar-*H*), 3.79 (m, 3 H, *CH*₃), 2.67 (t, ³J_{H,H} = 7.6 Hz, 2 H, Ar*CH*₂), 2.16-1.91 (m, 4 H, *CH*₂).

4-Bromo-3-(1H,1H,2H,2H,3H,3H-perfluorononyl)anisole 6. A mixture of **5** (10.20 g, 21.8 mmol), NBS (4.30 g, 24.0 mmol, 1.1 eq) in dry CH₃CN (80 mL) was stirring for 8 h at RT. Afterwards the solvent was distilled off at a rotatory evaporator. Carbon tetrachloride was added to the residue. The solid (succinimide) was filleted off and washed with carbon tetrachloride thoroughly, yield: 9.2 g (82.1 %); yellow oil; C₁₆H₁₂OBrF₁₃, M = 547 g/mol, ¹H-NMR (200 MHz; CDCl₃): δ / ppm = 7.43 (d, ³J_{H,H} = 8.6 Hz, 1H, Ar-*H*), 6.58 (d, ³J_{H,H} = 2.9 Hz, 1H, Ar-*H*), 5.67 (dd, ⁴J_{H,H} = 3.12 Hz, ³J_{H,H} = 8.8 Hz, 1H, Ar-*H*), 3.77 (s, 3H, *CH*₃), 2.77 (t, ³J_{H,H} = 7.43 Hz, 2H, Ar*CH*₂), 2.18-1.93 (m, 4H, *CH*₂).

4,4''-Dimethoxy-2,2''-bis(1H,1H,2H,2H,3H,3H-perfluorononyl)-*p*-terphenyl 7. Synthesized by Pd⁰ catalyzed Suzuki cross coupling as described in refs. ^{S9,S7} A mixture of **6** (3.00 g, 5.5 mmol), benzene-1,4-diboronic acid (0.40 g, 2.4 mmol), Pd(PPh₃)₄ (0.30 g), ethyleneglycoldimethylether (40 mL), and saturated NaHCO₃ solution (25 mL) was refluxed for 6 h under an argon atmosphere. After staying over night at RT, the precipitate was filtered, and dissolved in chloroform (50 mL). The solution was dried over Na₂SO₄, filtered through silica gel and the silica gel was washed thoroughly with chloroform (100 mL), the solvent was evaporated and the product was purified by preparative centrifugal thin layer chromatography (eluent: CHCl₃), yield: 2.2 g (92.2 %); yellow waxy solid;. C₃₈H₂₈O₂F₂₆, M = 1011 g/mol, ¹H-NMR (200 MHz; CDCl₃): δ / ppm = 7.46 (d, ³J_{H,H} = 8.8 Hz, 4H, Ar-*H*), 7.24 (m, 2H, Ar-*H*),

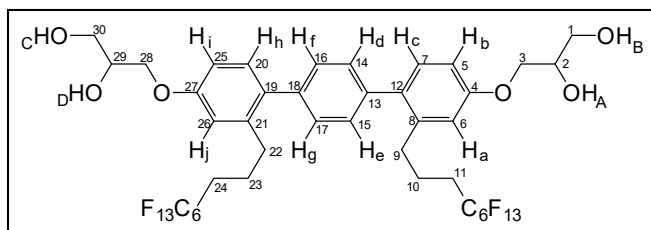
6.88 (m, 4H, Ar-*H*), 3.84 (s, 6H, 2 CH₃O), 2.71 (t, ³J_{H,H} = 7.43 Hz, 4H, CH₂Ar), 1.96-2.11 (m, 8H, CH₂CH₂CF₂).

2,2''-Bis(1H,1H,2H,2H,3H,3H-perfluorononyl)-*p*-terphenyl-4,4''-diol 8. Demethylation was performed using the method described in refs.^{S10,S7} **7** (2.20 g, 2.2 mmol) was dissolved in CH₂Cl₂ (30 mL), BBr₃ (0.50 mL, 4.9 mmol) was added and the solution was refluxed for 4 h. After stirring for 20 h at room temperature, water (30 mL) was carefully added, the solvent was distilled off, the residue was dissolved in diethyl ether (100 mL) and washed with saturated NaHCO₃ solution (2×30 mL), and dried over Na₂SO₄, the solvent was distilled off *in vacuo*. The product was purified by recrystallization from CHCl₃/MeOH = 5/2, v/v. yield: 0.8 g (38.5 %); yellow solid; mp: 175 °C; C₃₆H₂₄O₂F₂₆, M = 982 g/mol. ¹H-NMR (200 MHz; CDCl₃): δ / ppm = 7.25 (m, 4H, Ar-*H*), 6.99 (m, 2H, Ar-*H*), 6.67-6.73 (m, 4H, Ar-*H*), 2.64 (t, ³J_{H,H} = 8.2 Hz, 4H, 2 ArCH₂), 2.67-1.97 (m, 4H, 2 CH₂), 1.58 (m, 4H, 2 CH₂).

4,4''-Diallyloxy-2,2''-di(1H,1H,2H,2H,3H,3H-perfluorononyl)-*p*-terphenyl 9.

The etherification was performed as described in ref.^{S7} Allylbromide (0.2 mL, 2.0 mmol) was added under an argon atmosphere to a mixture of **8** (0.8 g, 0.9 mmol) and K₂CO₃ (0.2 g, 1.3 mmol) in dry CH₃CN (50 mL). The mixture was refluxed for 2 h (TLC). CH₃CN was evaporated *in vacuo*. Water (100 mL) and diethyl ether (100 mL) were added to the residue. The organic layer was separated, and the aqueous layer was extracted with diethyl ether (3×100 mL). The combined extracts were washed with H₂O (3×75 mL), dried over Na₂SO₄ and the solvent were evaporated *in vacuo*. Crude product was used for the next step, yield: 0.7 g (92.5 %); yellow solid; mp: 87 °C; C₄₂H₃₂O₂F₂₆, M = 1062 g/mol, ¹H-NMR (200 MHz; CDCl₃): δ / ppm = 7.31-7.15 (m, 6H, Ar-*H*), 6.81 (m, 4H, Ar-*H*), 6.17-5.98 (m, 2H, 2 CH=), 5.26-5.47 (m, 4H, 2 CH₂=), 4.55 (m, 4H, 2 CH₂O), 2.65 (t, ³J_{H,H} = 7.23 Hz, 4H, 2 ArCH₂), 1.98-1.72 (m, 8H, 2 CH₂CH₂).

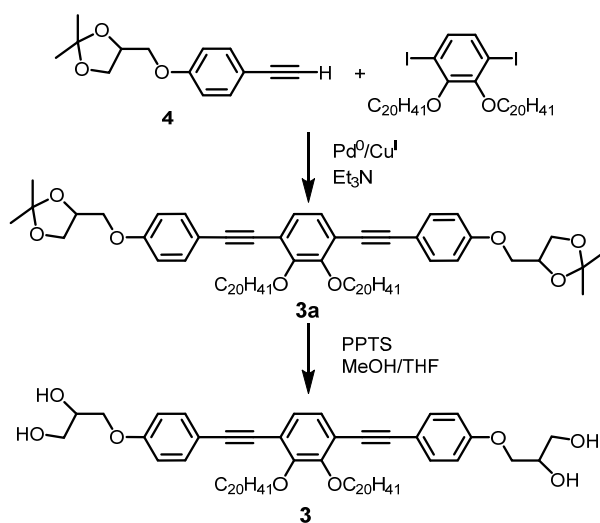
3-[4''-(2,3-Dihydroxypropoxy)-2,2''-bis(1H,1H,2H,2H,3H,3H-perfluorononyl)-*p*-terphenyl-4-yloxy]propane-1,2-diol 2



The dihydroxylation reaction was performed as described in refs.^{S11,S7} **9** (0.70 g, 0.6 mmol), and NMMNO (1.0 mL, 5.7 mmol of 60 % solution in water) were dissolved in acetone (25 mL). Osmium tetroxide (1.0 ml of a 0.004 M solution in *tert*-butanol) was added, and the solution

was stirred 2 h at RT. Afterwards, saturated aqueous Na₂SO₃ solution (5 mL) was added and the mixture was stirred for 30 min at RT. The mixture was filtered over a silica bed. The residue was carefully washed twice with acetone (50 mL), and the solvent was evaporated in *vacuo*. The residue was dissolved in ethyl acetate (100 mL). The solution was washed with 10 % aqueous H₂SO₄ (30 ml), saturated NaHCO₃ solution (30 mL) and H₂O (30 mL). The organic layer was dried over Na₂SO₄, and the solvent was evaporated in *vacuo*. Purification was conducted by column chromatography (eluent: CHCl₃/MeOH 9/1 v/v) and crystallization from CHCl₃/*n*-hexane 2/1, v/v, yield: 231 mg (33 %); C₄₂H₃₆O₆F₂₆, M = 1131 g/mol. **¹H NMR** (500 MHz, pyridine-*d*₅): δ/ppm = 7.54 (s, 4H, Aryl-*H*), 7.35 (d, ³J_{H,H} = 8.4 Hz, 2H, Aryl-*H*), 7.19 (d, ⁴J_{H,H} = 2.4 Hz, 2H, Aryl-*H*), 7.12 (dd, ³J_{H,H} = 8.4 Hz, ⁴J_{H,H} = 2.6 Hz, 2H, Aryl-*H*), 6.95 (s, 2H, *OH*), 6.55 (s, 2H, *OH*), 4.65 – 4.58 (m, 4H, OCH₂, OCH), 4.54 (dd, *J* = 9.2, 6.0 Hz, 2H, OCH₂), 4.30 (m, 4H, OCH₂), 2.90 – 2.80 (m, 4H, OCH₂), 2.13 – 1.97 (m, 4H, CH₂), 1.90 – 1.80 (m, 4H, CH₂CF₂). **¹³C NMR** (126 MHz, pyridine) δ 159.19, 140.19, 139.84, 134.22, 131.52, 129.48, 115.87, 112.60 (Aryl-*C*), 71.32 (OCH), 70.74 (CH₂), 64.13 (OCH₂), 32.55 (Aryl-CH₂), 30.21 (t, ²J_{C,F} = 18.4 Hz, CH₂CF₂), 21.54 (CH₂). **¹⁹F-NMR** (470 MHz, pyridine-*d*₅): δ/ppm = -80.99 (t, *J* = 9.8 Hz, CF₃), -113.87 – -114.08 (m, CF₂), -121.94 (s, CF₂), -122.92 (s, CF₂), -123.41 (s, CF₂), -126.01 – -126.41 (m, CF₂). **HRMS** (m/z): [M]⁺Li⁺ calcd. for C₄₂H₃₆F₂₆O₆Li, 1137.2252; found 1137.2254. Analysis calcd. for C₄₂H₃₆O₆F₂₅ · H₂O (for determination of crystal water, see ref. S2) C 43.92, H 3.33 %; found: C 43.93, H 3.67 %.

S4.3. Synthesis of compound 3



Scheme S2: Synthesis of compound 3.

3,6-Diiodo-1,2-dieicosyloxybenzene: Synthesized according to ref.^{S4} from 3,6-diiodocatechol (250 mg, 0.69 mmol), 1-bromoeicosane (550 mg, 1.52 mmol), K_2CO_3 (960 mg, 6.90 mmol), Bu_4NI (10 mg, 0.03 mmol) in DMF (30 mL). purification by column chromatography (eluent: *n*-hexane/ $CHCl_3$ = 4/1), colorless solid, $C_{46}H_{84}I_2O_2$, $M = 922.97$ g/mol, yield: 230 mg (37%), mp. 84 °C, ^1H-NMR ($CDCl_3$, 400 MHz): δ / ppm = 7.22 (s, 2H, Aryl-*H*), 3.98 (t, $^3J_{H,H} = 6.7$ Hz, 4H, OCH_2), 1.89 – 1.77 (m, 4H, CH_2), 1.52 – 1.44 (m, 4H, CH_2), 1.41 – 1.21 (m, 64H, CH_2), 0.89 (t, $^3J_{H,H} = 6.8$ Hz, 6H, CH_3).

1,4-Bis{4-[(2,2-dimethyl-1,3-dioxolane-4-yl)methoxy]phenylethynyl}-2,3-dieicosyloxybenzene (3a): Synthesized by Sonogashira cross coupling as described in ref.^{S5} A mixture of 3,6-diiodo-1,2-dieicosyloxybenzene (210 mg, 0.23 mmol) and **4** (120 mg, 0.50 mmol) was dissolved in dry Et_3N (50 mL). After degassing with argon for 30 min [$Pd(PPh_3)_4$] (15 mg, 0.01 mmol) and CuI (5 mg, 0.01 mmol) were added and the mixture was refluxed for 6 h. After removing the solvent the obtained residue was purified by column chromatography (eluent: $CHCl_3$), yellowish solid, $C_{74}H_{114}O_8$, $M = 1132$ g/mol, Yield: 180 mg (69%), mp. 63 °C, ^1H-NMR ($CDCl_3$, 400 MHz): δ / ppm = 7.46 (d, $^3J_{H,H} = 8.9$ Hz, 4H, Aryl-*H*), 7.15 (s, 2H, Aryl-*H*), 6.89 (d, $^3J_{H,H} = 8.9$ Hz, 4H, Aryl-*H*), 4.53 – 4.44 (m, 2H, OCH), 4.22 – 4.11 (m, 6H, OCH_2), 4.11 – 4.04 (m, 2H, OCH_2), 4.01 – 3.93 (m, 2H, OCH_2), 3.91 (dd, $^3J_{H,H} = 8.5$, $^3J_{H,H} = 5.8$ Hz, 2H, OCH_2), 1.89 – 1.72 (m, 4H, CH_2), 1.60 – 1.48 (m, 4H, CH_2), 1.47 (s, 6H, $OC(CH_3)_2$), 1.41 (s, 6H, $OC(CH_3)_2$), 1.25 (s, 64H, CH_2), 0.88 (t, $^3J_{H,H} = 6.9$ Hz, 6H, CH_3).

1,4-Bis[4-(2,3-dihydroxypropoxy)phenylethynyl]-2,3-dieicosyloxybenzene (3).

The cleavage of the isopropylidene protecting group was performed as described in ref.^{S12} A mixture of **3a** (180 mg, 0.16 mmol.) and PPTS (20 mg, 0.06 mmol) was dissolved in THF/MeOH (1:1, 60 mL) and stirred at 50 °C for 12 h. After finishing the reaction the solvent was removed and the residue solved in DCM. The organic layer was washed with NaHCO₃ solution (3 x 50 mL), water and brine. After drying over Na₂SO₄ the solvent was removed and the residue purified with column chromatography (eluent: CHCl₃/MeOH = 9:1) and recrystallisation from MeOH/THF, white solid, C₆₈H₁₀₆O₈, *M* = 1052 g/mol, Yield: 90 mg (53%), mp. 98 °C, ¹H-NMR (pyridine-d₅, 400 MHz): δ / ppm = 7.74 (d, ³J_{H,H} = 8.8 Hz, 4H, Aryl-*H*), 7.42 (s, 2H, Aryl-*H*), 7.16 (d, ³J_{H,H} = 8.8 Hz, 4H, Aryl-*H*), 4.62 – 4.50 (m, 4H, OCH₂), 4.49 – 4.38 (m, 6H, OCH₂, OCH), 4.24 (d, ³J_{H,H} = 5.0 Hz, 4H, OCH₂), 2.11 – 1.96 (m, 4H, CH₂), 1.70 (m, 4H, CH₂), 1.53 – 1.18 (m, 64H, CH₂), 0.89 (t, ³J_{H,H} = 6.9 Hz, 6H, CH₃). ¹³C NMR (pyridine-d₅, 126 MHz): δ / ppm = 160.01, 153.99, 133.24, 127.87, 119.70, 115.36, 115.20 (Aryl-*C*), 95.56, 85.21 (C≡C), 74.28, 71.09, 70.84 (OCH₂), 64.01 (OCH), 31.86, 30.66, 29.79, 29.78, 29.76, 29.74, 29.73, 29.66, 29.65, 29.35, 26.40, 22.67 (CH₂), 14.01 (CH₃). HRMS (m/z): [M]⁺Cl⁻ calcd. for C₆₈H₁₀₆O₈Cl, 1085.7571; found 1085.7574. Analysis: calcd. for C₆₈H₁₀₆O₈: C 77.67, H 10.16%; found: C 77.87, H 10.14 %

S5. Supporting Discussion and Calculations

S5.1 Difference between molecular length and *a*_{cub}

For both compounds **2** and **3** the cubic lattice parameter is about 20% larger than the single molecular length. The reason is the space required by the spheres involving the glycerol groups, which is shown below by some rough estimations. There is one glycerol micelle per unit cell of the *Pm3m* lattice, i.e. its volume (*V*_{mic}) corresponds to *V*_{mic} = *n*_{cell} x 2*V*_{gly}. In the case of compound **3** *V*_{mic} = 26.5 x 0.212 nm³ = 5.62 nm³. Assuming a spherical shape, the diameter of the sphere would be *d*_{mic} = ³√(6*V*_{gly}/π) = 2.2 nm. This adds to the length of the 1,4-bis(phenylethynyl)benzene core unit with *L*_{core} = 1.8 nm, giving a side length of the cube of *a*_{calc} = 4.0 nm. The measured parameter *a*_{cub} = 3.6 nm is the average between the stretched molecular length (*L*_{mol} = 3.1 nm) and the above calculated side length (*a*_{calc} = 4.0 nm). The probable reason is, that the limitations given by the well defined distance provided by the rod-like core structure does not allow the formation of perfect spheres and the system adjusts to a compromise between the requirements of the well defined and restricted core length and the volume required by the attached polar spheres.

Related data were obtained for compound **2**: $V_{\text{mic}} = 19.3 \times 0.212 \text{ nm}^3 = 4.1 \text{ nm}^3$ with $d_{\text{mic}} = 2.0 \text{ nm}$; $L_{\text{core}} = 1.3 \text{ nm}$, $a_{\text{calc}} = 2.0 + 1.3 = 3.3 \text{ nm}$; again a_{calc} is the average between $L_{\text{mol}} = 2.5 \text{ nm}$ and $a_{\text{cub}} = 2.9 \text{ nm}$

The molecular lengths were determined with space-filling CPK models and were measured for the most stretched conformation between the ends of the primary OH groups at both ends. In a similar manner the core length was determined between the ends of the aromatic cores. The molecular volumes were estimated with Immirzies crystal volume increments,^{S3} corrected by the factor 1/0.893 to consider the reduced packing density in the LC state.

S5.2 Packing of R_F chains in the *Pm3m* phase of compound 2

As noted in the main text, there is a reduced packing density for the R_F segments in the center of the unit cell. Due to the weak polarizability of perfluorinated alkyl chains, there is only weak intermolecular interactions between them,^{S13} leading to a reduced contribution of ΔH to ΔG . Therefore, the reduced packing density does not change ΔH significantly and simultaneously provides a gain of entropy due to an increased chain mobility, which can compensate the loss in ΔH . In contrast, for non—fluorinated alkyl chains the reduction of the packing density is more difficult because the stronger dispersion interactions between the highly polarizable alkyl chains leads to an increased importance of ΔH and a compensation by increasing $T\Delta S$ is less efficient.

S6. Additional NMR spectra

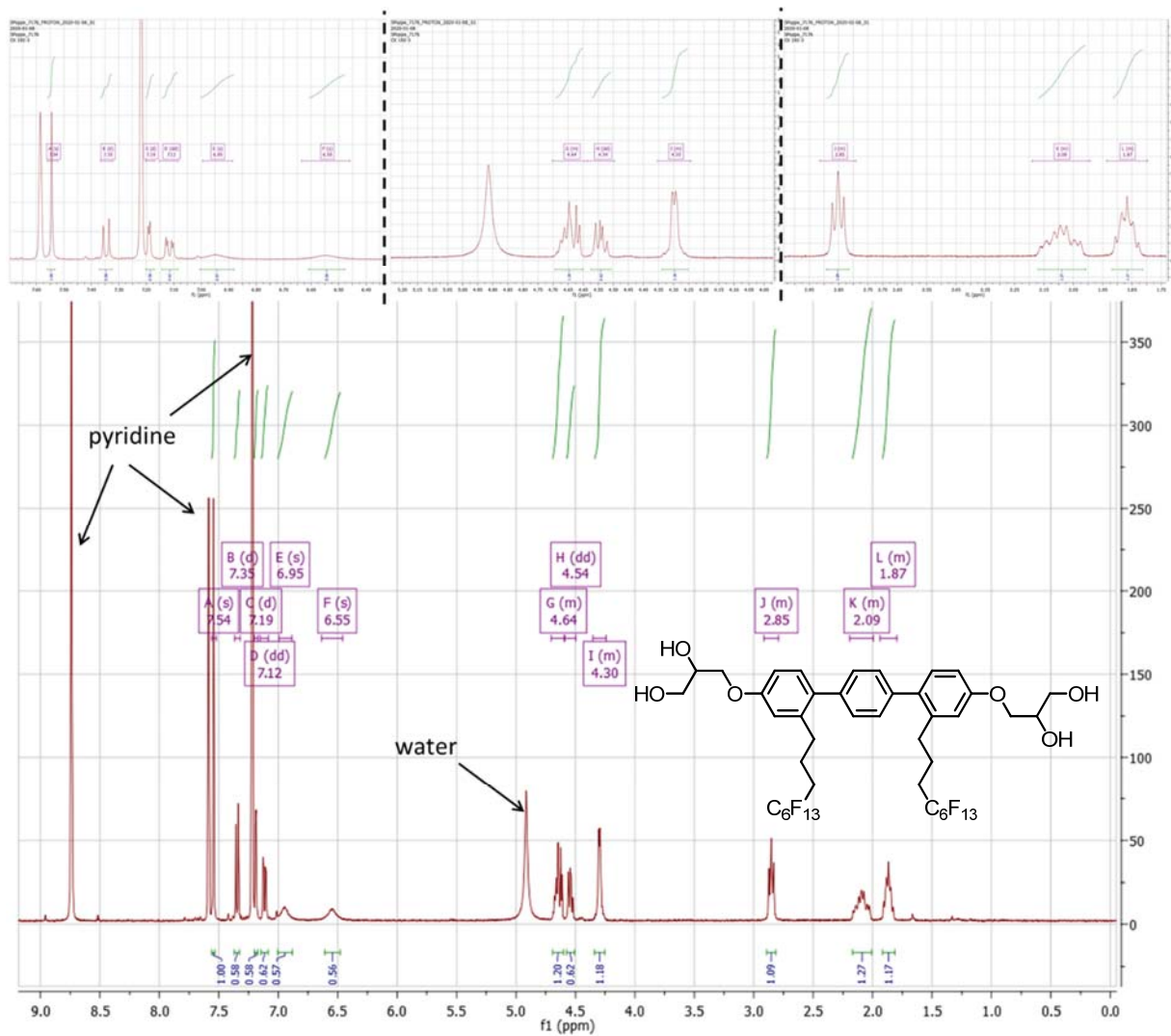


Figure S7 (8). $^1\text{H-NMR}$ spectrum of **2** (500 MHz; pyridine-d_5).

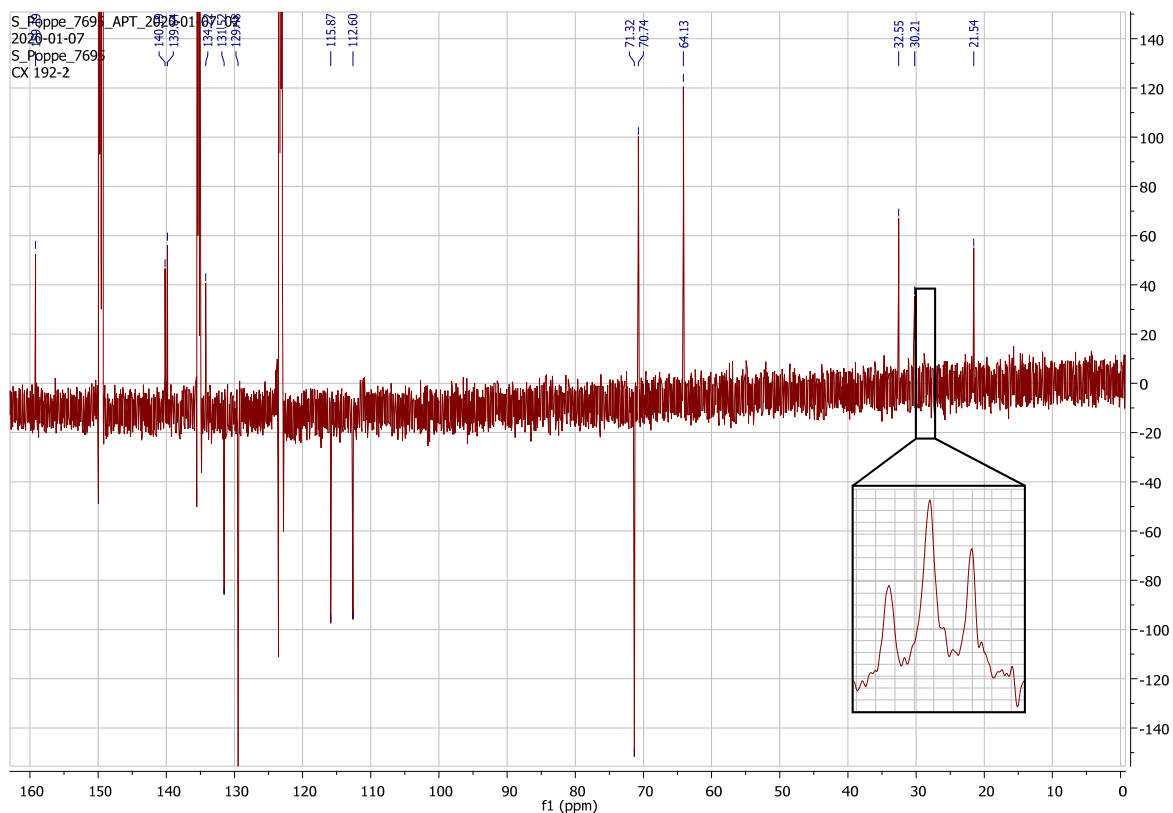


Figure S8. ^{13}C -NMR spectrum of **2** (126 MHz; pyridine- d_5).

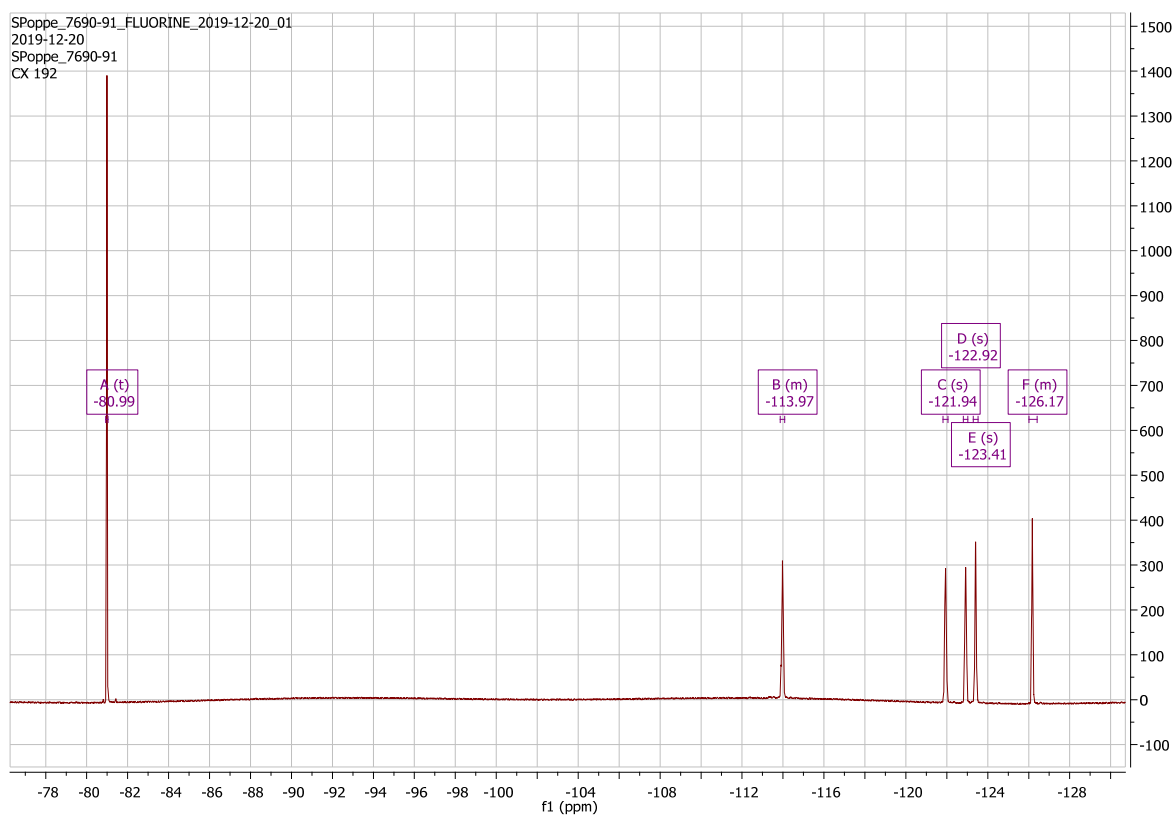


Figure S9. ^{19}F -NMR spectrum of **2** (470 MHz; pyridine- d_5).

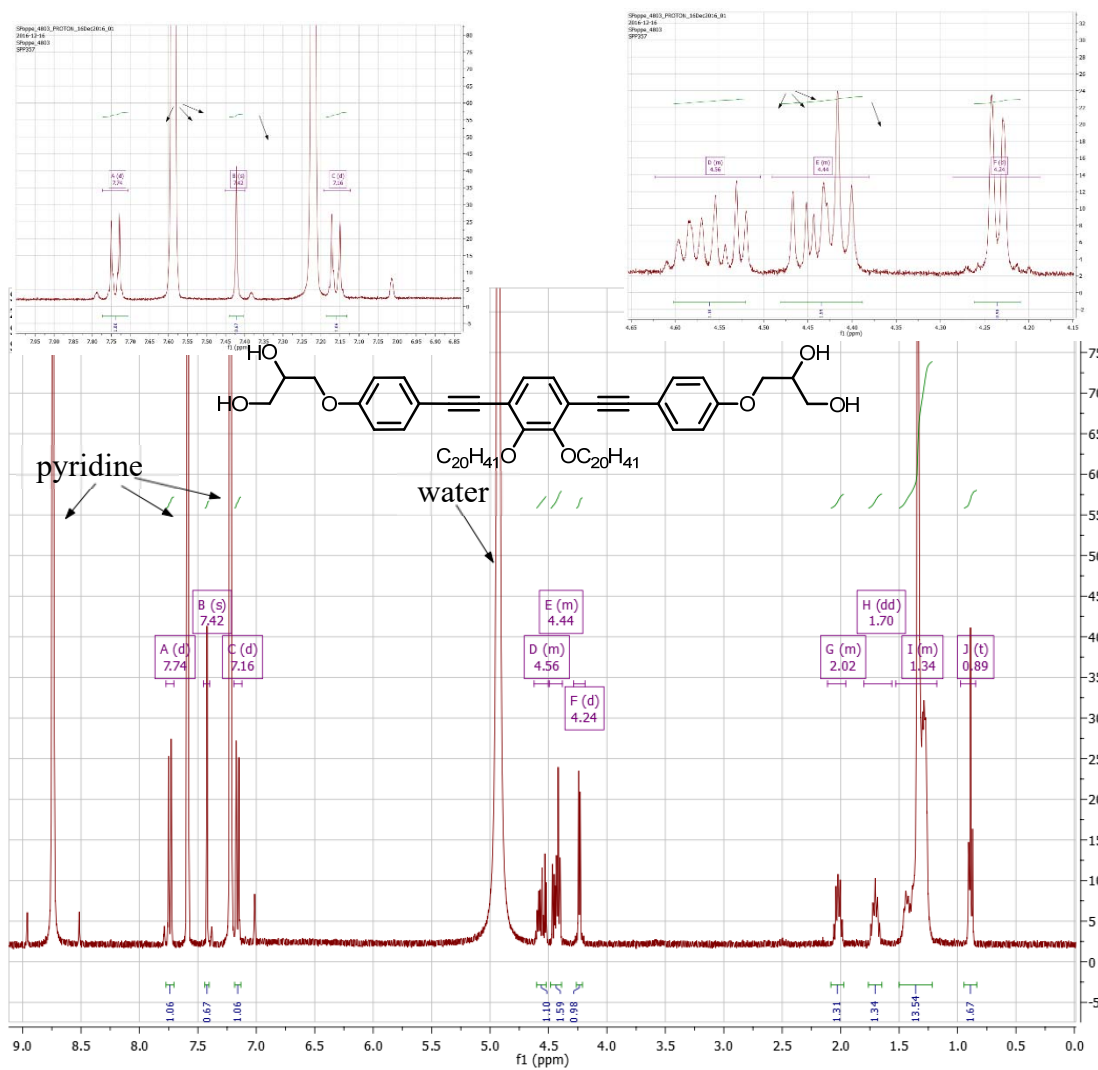


Figure S10. $^1\text{H-NMR}$ spectra of **3** (400 MHz; pyridine- d_5).

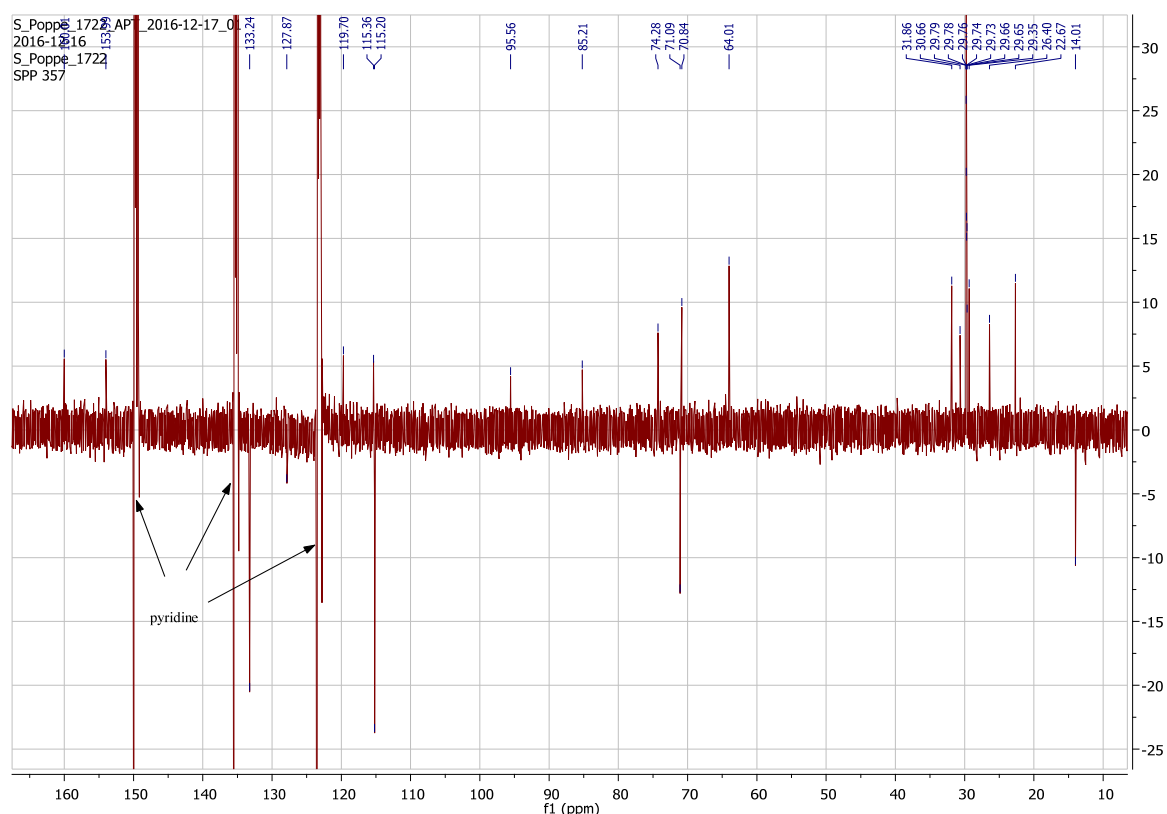


Figure S11. ^{13}C -NMR spectra of **3** (126 MHz; pyridine- d_5).

S7. References

- S1 Joachimi, D.; Lattermann, G.; Schellhorn, M.; Tschierske, C.; Zugenmaier, P. Investigation of the Crystal Structure of Two Amphiphilic Diols. *Liqu. Cryst.* **1995**, *18*, 303-307.
- S2 Dunkel, R.; Hahn, M.; Borisch, K.; Neumann, B.; Rüttinger, H.-H.; Tschierske, C. Determination of the Water Content of Amphiphilic Liquid Crystals by Coulometric Karl Fischer Titration. *Liqu. Cryst.* **1998**, *24*, 211- 213.
- S3 Immirzi, A.; Perini, B. Prediction of Density in Organic Crystals. *Acta Cryst.* **1977**, *A33*, 216-218.
- S4 Zhu, Z.; Swager, T. M. Conjugated Polymers Containing 2,3-Dialkoxybenzene and Iptycene Building Blocks. *Org. Lett.* **2001**, *3*, 3471-3474.
- S5 Poppe, S.; Poppe, M.; Ebert, H.; Prehm, M.; Chen, C.; Liu, F.; Werner, S.; Bacia, K.; Tschierske, C. Effects of Lateral and Terminal Chains of X-Shaped Bolapolyphiles with Oligo(phenylene ethynylene) Cores on Self-Assembly Behaviour. Part 1: Transition between Amphiphilic and Polyphilic Self-Assembly in the Bulk. *Polymers* **2017**, *9*, 471.
- S6 Kölbel, M.; Beyersdorff, T.; Cheng, X.; Tschierske, C.; Kain, J.; Diele, S. Design of Liquid Crystalline Block Molecules with Nonconventional Mesophase Morphologies: Calamitic Bolaamphiphiles with Lateral Alkyl Chains. *J. Am. Chem. Soc.* **2001**, *123*, 6809-6818.
- S7 Cheng, X.; Prehm, M.; Das, M. K.; Kain, J.; Baumeister, U.; Diele, S.; Leine, D.; Blume, A.; Tschierske, C. Calamitic Bolaamphiphiles with (Semi)Perfluorinated Lateral Chains: Polyphilic Block Molecules with New Liquid Crystalline Phase Structures. *J. Am. Chem. Soc.* **2003**, *125*, 10966-10977.

-
- S8 Johansson, G.; Percec, V.; Ungar, G.; Zhou, J. P. Fluorophobic Effect in the Self-Assembly of Polymers and Model Compounds Containing Tapered Groups into Supramolecular Columns. *Macromolecules*, **1996**, *29*, 646-660.
- S9 Miyaura, N.; Yanagi, T.; Suzuki, A. The Palladium-Catalyzed Cross-Coupling Reaction of Phenylboronic Acid with Haloarenes in the Presence of Bases. *Synth. Commun.* **1981**, *11*, 513-519.
- S10 a) Demuyck, M.; De Clercq, P.; Vandewalle, M. (±)-Hysterin: revised structure and total synthesis. *J. Org. Chem.* **1979**, *44*, 4863-4866; b) Grieco, P. A.; Nishizawa, M.; Oguri, T.; Burke, S. D.; Marinovic, N., Sesquiterpene Lactones: Total Synthesis of (±)-Vernolepin and (±)-Vernomenin. *J. Am. Chem. Soc.* **1977**, *99*, 5773-5780.
- S11 van Rheenen, V.; Cha, D. Y.; Hartley, W. M. Catalytic Osmium Tetroxide catalytic Oxidation of Olefins: *cis*-1,2-Cyclohexanediol. *Org. Synth.* **1979**, *58*, 43.
- S12 van Rijsbergen, R.; Anteunis, M.J.O.; de Bruyn, A. Selective Removal of the Isopropylidene Group in 4-O-Protected 1,6-Anhydro-2,3-O-Isopropylidene-β-D-Mannopyranose and the Conformational Impact of it. *J. Carbohydr. Chem.* **2006**, *2*, 395-404.
- S13 Tschierske, C. Fluorinated Liquid Crystals: Design of Soft Nanostructures and Increased Complexity of Self-Assembly by Perfluorinated Segments. *Top. Curr. Chem.* **2012**, *318*, 1-108.